



Sediment supply and relative size distribution effects on fine sediment infiltration into immobile gravels

John K. Wooster,¹ Scott R. Dusterhoff,¹ Yantao Cui,¹ Leonard S. Sklar,² William E. Dietrich,³ and Mary Malko¹

Received 8 December 2006; revised 19 October 2007; accepted 12 December 2007; published 21 March 2008.

[1] We present results and analyses from flume experiments investigating the infiltration of sand into immobile clean gravel deposits. Three runs were conducted, each successive run with the same total sediment feed volume, but a 10-fold increase in sand feed rate. The highest sand feed rate produced less sand infiltration into the subsurface deposits than the other two runs, which had approximately equivalent amounts of sand infiltration. Experimental data, combined with simple geometric relations and physical principles, are used to derive two relations describing the saturated fine sediment fraction in a gravel deposit and the vertical fine sediment fraction profile resulting from fine sediment infiltration. The vertical fine sediment fraction profile relation suggests that significant sand infiltration occurs only to a depth equivalent to a few median grain diameters of the bed material.

Citation: Wooster, J. K., S. R. Dusterhoff, Y. Cui, L. S. Sklar, W. E. Dietrich, and M. Malko (2008), Sediment supply and relative size distribution effects on fine sediment infiltration into immobile gravels, *Water Resour. Res.*, 44, W03424, doi:10.1029/2006WR005815.

1. Introduction

[2] Understanding the mechanics of fine sediment infiltration into gravel deposits is critical for assessing the biologic and economic impacts from upstream anthropogenic and natural fine sediment releases in rivers. Riverine gravel deposits of appropriate grain sizes provide important spawning habitat for salmonids in the Pacific Northwest of the US and elsewhere [Kondolf and Wolman, 1993]. Adult salmonids bury their eggs into gravel deposits, which then incubate in the substrate for up to five months before hatching [Groot and Margolis, 1991]. Many factors may affect the survival of the salmonid eggs during this long hatching period, including excessive infiltration of fine sediment which may result in decreased egg survival due to reduced intra-gravel flow that brings oxygen to the embryos [e.g., Cooper, 1965; Koski, 1966; Greig et al., 2005a, 2005b, 2007; Sear et al., 2005] and difficulties for hatchlings (alevins) to emerge from the gravel deposit if they hatch successfully [Einstein, 1968; Phillips et al., 1975; Hausel and Coble, 1976]. In addition to negative influences on fish embryo survival, excessive fine sediment infiltration may also reduce invertebrate productivity, which serves as the primary food source for salmonids and other fish species [Gammon, 1970; Brusven and Prather, 1974; Bjornn et al., 1977]. There are also potential important economic ramifications associated with increased fine sed-

iment infiltration into river bed sediments. For example, an increase in fine sediment infiltration may result in a decreased efficiency for infiltration wells that draw water directly beneath the river bed, imposing higher costs for pumping operations. This is currently a major issue in the ongoing planning and design of the removal of two dams on the Elwha River, Washington (Blair Greimann, personal communication, 6 July 2006).

[3] Increased fine sediment infiltration into a gravel river bed can occur as a result of an increase in fine sediment supply. Such increases in sediment supply may come from chronically accelerated erosion due to land use [e.g., Walling, 1999] or from relatively short-term events such as landslides [e.g., Sutherland et al., 2002], accidental sediment release from reservoirs [e.g., Rathburn and Wohl, 2001], and sediment releases following dam removal [e.g., Cui and Wilcox, 2008]. With the continued decline in salmonid populations that may be at least partially attributed to increased fine sediment production and subsequent deposition and infiltration, a better understanding of the mechanisms of fine sediment infiltration into gravel-bedded channels is becoming increasingly important.

[4] Several flume and field studies have previously investigated fine sediment infiltration into gravel deposits. One of the first studies of fine sediment infiltration was conducted by Einstein [1968] in a recirculating flume with a clean (i.e., initially void of any fine sediment) gravel channel bed set to a thickness of 1 to 2.7 times the coarsest gravel diameter. By feeding ground quartz (ranging from 0.0035 to 0.03 mm in diameter) over the clean gravel, Einstein [1968] observed that fine sediment settles first at the bottom of the flume in the interstices of gravel deposits and gradually fills the interstices upward. In a flume filled with 4.5- to 50-mm diameter gravel and feeding 0.2-mm and 0.5-mm diameter sand for infiltration, Beschta and

¹Stillwater Sciences, Berkeley, California, USA.

²Department of Geosciences, San Francisco State University, San Francisco, California, USA.

³Department of Earth and Planetary Science, University of California, Berkeley, California, USA.

Jackson [1979] observed that fine sediment infiltrated to a depth of approximately 10 cm, or approximately twice the diameter of the coarsest bed material. *Beschta and Jackson* [1979] also observed that there was less than 8% sand in the deposit following infiltration of 0.5-mm sand but this number increased to 15% using the 0.2-mm sand for infiltration. This observation suggests that the size ratio of coarse sediment (i.e., framework of the sediment deposit) to fine sediment (i.e., infiltrating sediment) is important in determining the amount of fine sediment infiltration.

[5] The field study of *Frostick et al.* [1984] examined fine sediment infiltration into gravel deposits with different bed material (subsurface) grain sizes while maintaining the same grain size for the surface layer. Their observations indicated more fine sediment infiltrated into the coarser subsurface deposits than into the finer subsurface deposits. While *Frostick et al.* [1984] proposed that higher fine sediment infiltration into the coarser subsurface might be a result of a lower surface-to-subsurface grain size ratio, the experiments of *Beschta and Jackson* [1979] suggest that the coarse sediment (i.e., bed material) to finer infiltrating sediment grain size ratio was the predominant parameter affecting infiltration differences between varying subsurface deposits.

[6] Based on results using recirculating and non-recirculating flumes, *Diplas and Parker* [1985] concluded that an immobile gravel bed would eventually become saturated with fine sediment as long as fine sediment particles were available in the water column, irrespective of the fine sediment concentration in the water column. *Diplas and Parker* [1985] also confirmed *Beschta and Jackson's* [1979] observation that the ratio of fine sediment to bed material grain sizes is an important parameter affecting the amount of fine sediment infiltration.

[7] Observations of fine sediment infiltration in the field have also shown that fine sediment infiltration occurs to a limited depth within gravel beds. On the basis of field experiments from three streams in northern California, *Lisle* [1989] observed that fine sediment infiltration decreases with increasing bed load transport and proposed that sand trapped in the interstices of the top several centimeters of the deposit formed a seal that impeded deeper infiltration of much finer sediments. On the basis of flume studies, *Carling* [1984] and *Schälchli* [1992] also concluded that fine sediment only infiltrates into a coarser bed to a limited depth.

[8] Recent studies have shown the importance of the variability in bed particle sizes in the dynamics of fine sediment infiltration into gravel beds. By analyzing fine sediment content from a set of large-scale flume experiments presented by *Seal et al.* [1995] and *Toro-Escobar et al.* [1996], *Cui and Parker* [1998] found that the fine sediment fraction (FSF hereafter) in gravel deposits is negatively correlated to the standard deviation of particle diameters within the gravel deposit. *Cui and Parker* [1998] hypothesized that the standard deviation of a clean gravel deposit is a surrogate measure for pore space available for fine sediment to infiltrate, and the amount of fine sediment that can infiltrate into the deposit is directly correlated with the available pore space.

[9] In an effort to explain the observations of fine sediment infiltration into gravel beds, researchers have developed theoretical and probabilistic models. *Lauck*

[1991] provided a hypothetical process for sand infiltration and developed a stochastic model to qualitatively explain the observations by previous researchers [e.g., *Einstein*, 1968; *Beschta and Jackson*, 1979]. The *Lauck* [1991] model reproduced the general observations of *Einstein* [1968] that fine sediment fills the pores from the bottom up when the size ratio of bed material to fine sediment was large and the bed material was shallow. It also reproduced the general observation from other studies that fine sediment can only infiltrate a finite depth if the bed material is sufficiently thick [e.g., *Beschta and Jackson*, 1979; *Frostick et al.*, 1984; *Carling*, 1984; *Lisle*, 1989; *Schälchli*, 1992]. To further test the *Lauck* [1991] model, *Rohn* [1997] collected fine sediment infiltration data by submerging glass beads and naturally rounded pebbles into hot gelatin solutions and then raining fine sediment into the solution. *Rohn's* [1997] data compared to *Lauck's* [1991] model indicated that the model performed well for non-uniform bed material but poorly for uniform bed material. *Cui et al.* [2008] developed a theory that describes the processes of fine sediment infiltration based on the process outlined by *Lauck* [1991]. On the basis of this theory, the highest possible FSF resulting from fine sediment infiltrating an immobile clean gravel deposit is an exponential decay function with depth into the bed material, implying that significant fine sediment infiltration occurs only to a limited depth.

[10] Building upon previous research, we designed a series of three flume runs to better understand the dynamics of fine sediment infiltration into immobile gravel deposits. In particular, we examined the effects of the grain-size distributions of the coarse bed material and the infiltrating fine sediment, and the influence of feed rate and duration of fine sediment feed during the infiltration process. On the basis of experimental results and simple geometric relations between the bed material and infiltrating fine sediments, semi-empirical relations (i.e., relations based partially on physical principles and partially on experimental data) were developed to describe (1) the saturated FSF in a coarse sediment deposit and (2) the vertical profile of infiltrated fine sediment into an immobile clean gravel deposit. These relations explain many of the observations from earlier studies [e.g., *Einstein*, 1968; *Beschta and Jackson*, 1979; *Frostick et al.*, 1984] within a physically rigorous framework.

2. Overview of the Experiments

[11] The experimental runs were conducted in a flume at the Richmond Field Station (RFS), University of California. The flume is 28 m long, 0.86 m wide and 0.9 m deep, and is equipped with sediment feeders, acoustic and laser beam scanners that measure detailed water surface profiles and sub-aqueous and sub-aerial bed topography, and continuous sediment-flux measurement equipment (Figure 1a). The three experimental runs were designed with the following considerations: (a) the combination of bed slope, water discharge, and bed material grain-size distributions should result in minimal transport of bed material (i.e., the experiments were conducted on a bed that was essentially immobile at the experimental discharge), for reasons that will be discussed later; (b) the spread and size range of bed material grain-size distributions should be maximized in order to

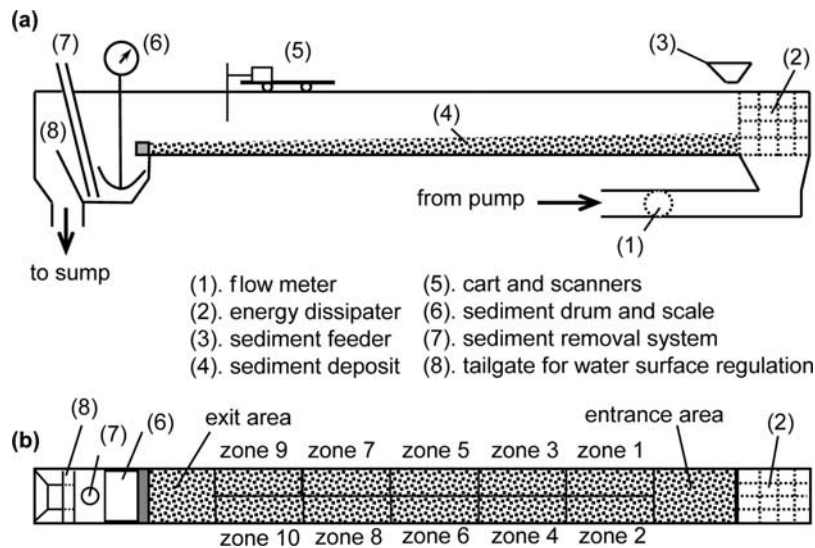


Figure 1. (a) Schematic diagram of the flume and associated equipment; and (b) plan view of the flume, showing the ten bed material zones used in the infiltration experiments. Diagrams are not to scale.

develop relations between fine sediment infiltration and bed material grain-size distributions; and (c) the majority of introduced fine sediment should move as bed load. The channel slope was set at 0.004 and a constant water discharge of 40 l/s was used for all the three experimental runs.

[12] The experimental section of the flume bed was located between 5 m from the flume entrance and 4.75 m upstream of the downstream weir, and was divided into 10 equal dimensioned zones with a length of 3.65 m and a width of 0.43 m (Figure 1b). Nine bed-material mixtures were produced by combining different ratios of five base sediments. The sediment mixture with the smallest median size was then placed in zone 9, one of the downstream-most zones, so that it would not transport into the other zones if the bed material was mobilized. The other eight mixtures were then randomly placed into zones 1 through 8. The sediment placed in zone 1 was also placed in zone 10 as a replicate in order to compare potential differences in infiltration due to longitudinal position of experimental zones and proximity to the sediment feed. The nine grain-size distributions are shown in Figure 2 and their geometric mean grain sizes and geometric standard deviations (see *Cui et al.* [1996] for the definition and calculation of geometric mean and geometric standard deviation) are listed in Table 1. Because of the varying grain-size distributions in different zones, it was not possible to create an initial equilibrium channel bed by feeding coarse sediment, as each zone would require different sediment feed rates and grain-size distributions to achieve an equilibrium state. Because of these limitations associated with varying grain-size distributions throughout the flume, we designed the experimental parameters so that there would be minimal bed degradation, even without coarse sediment feed.

[13] Typically a surface layer coarser than the subsurface material forms in a gravel-bedded river [e.g., *Parker and Sutherland*, 1990]. In an effort to replicate this process, we placed a coarser surface layer in eight of the ten zones. In the remaining two zones (4 and 6), the bed material was fairly uniform and no coarse surface layers were placed. The

surface grain-size distributions for the eight zones were determined by combining the surface-based bed load equation of *Parker* [1990] with the exchange function of *Hoey and Ferguson* [1994] and *Toro-Escobar et al.* [1996], which links the grain-size distribution of subsurface sediment with those in the bed load and surface layer (Table 1). A surface layer with a thickness of approximately 2 cm, which is equivalent to the coarsest particle size used for the experiment, was placed on top of the approximately 14-cm-thick subsurface bed, forming a deposit approximately 16 cm in total depth. Beneath the 16-cm experimental bed was sediment of similar size from previous experiments. After each run, the 16-cm experimental bed was completely excavated and new surface and subsurface material placed for subsequent experimental runs following the same procedure.

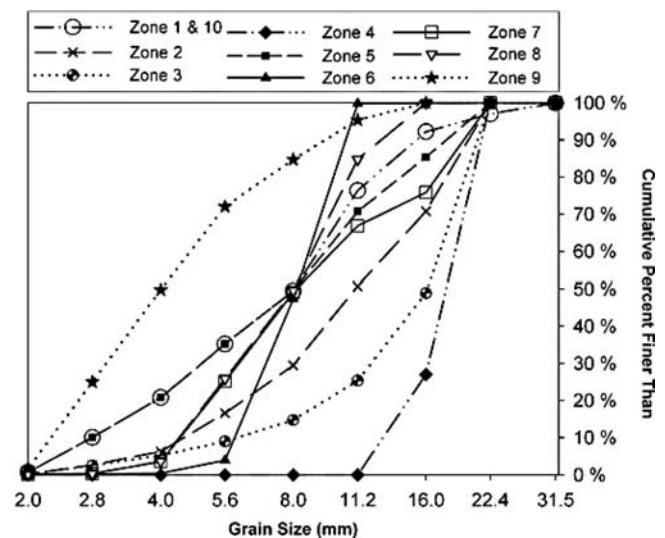


Figure 2. Bed material grain size distributions for the ten zones used in the infiltration experiments.

Table 1. Target Bed Material and Surface Layer Geometric Mean Grain Sizes and Geometric Standard Deviations for the Ten Zones Used in the Three Experimental Runs^a

Zone Number		1 and 10	2	3	4	5	6	7	8	9
Subsurface bed material	geometric mean, mm	7.0	10.2	13.1	17.2	7.3	7.9	8.8	7.6	4.2
	geometric standard deviation	1.82	1.74	1.67	1.17	1.90	1.23	1.72	1.46	1.65
Surface layer	geometric mean, mm	9.2	12.9	15.6	17.2	10.6	7.9	12.1	8.4	5.3
	geometric standard deviation	1.65	1.56	1.37	1.17	1.85	1.23	1.62	1.43	1.70

^aSampled geometric mean and geometric standard deviation values for individual sediment cores had local variations and are slightly different from the target values given in this table. Analyses conducted in the paper applied the measured geometric mean and geometric standard deviation values from each sediment core unless specified otherwise.

[14] After manually placing the sediment into the flume, we introduced flow and fine sediment feed to investigate fine sediment infiltration into the clean gravel deposits. The fine sediment used for infiltration was well-sorted fine sand with a geometric mean diameter of 0.35 mm and a geometric standard deviation of 1.24. Trial experiments indicated that the majority of the fine sand was transported as bed load with very little suspension at a discharge of 40 l/s. In order to finalize an appropriate fine sediment feed rate for Run 1, a 30-min trial run was conducted with a fine sediment feed rate of 0.048 kg/min (fed with a screw feeder at the flume entrance), and we determined that this feed rate was too low to completely saturate the gravel bed with fine sediment in a reasonable amount of time. The fine sediment feed rate was then increased by approximately a factor of 4.5 to 0.209 kg/min (fed with a screw feeder at the flume entrance) to start Run 1. Run 1 was terminated once observations indicated that there was minimal additional fine sediment infiltration and the bed material was saturated throughout the length of the flume (discussed later), which occurred after 100 h of fine sediment feed (Table 2).

[15] For Run 2, the fine sediment feed rate was increased by a factor of 10, relative to Run 1, to a feed rate of 2.09 kg/min (fed with a screw feeder at the flume entrance), and fine sediment was fed for 10 h so that the same volume of fine sediment was introduced to the flume as in Run 1. Following the termination of fine sediment feed in Run 2, we continued the water discharge of 40 l/s for three hours without fine sediment feed in order to transport the fine sediment deposits on the channel surface to the flume outlet so that approximately the same volume of fine sediment passed throughout the flume length. Although running water without the fine sediment feed transported fine sediment deposits that buried the gravel surface, it should not have resulted in a depletion of fine sediment infiltrated into the subsurface based on the observations of *Diplas and Parker* [1985] who noted that fine sediment in the inter-

stices of a gravel deposit can only be entrained if the coarse sediment is mobilized. Similar to Run 2, the fine sediment feed rate for Run 3 was increased by an additional factor of 10 to 20.9 kg/min (fed manually at approximately 2 m downstream of the flume entrance with buckets) and fine sediment was fed for one hour (Table 2). Following the termination of fine sediment feed in Run 3, the 40 l/s water discharge continued for 2.5 h. Because we did not initially envision the necessity of running clean water for Runs 2 and 3, Run 1 was terminated without running clean water. However, at the termination of fine sediment feed in Run 1 only a small fraction of the total volume of introduced fine sediment had not transport over the entire length of the flume due to the 100 h of run time. In Runs 2 and 3, a significant volume of the introduced fine sediment remained in the flume at the termination of the sediment feed which necessitated the additional clean water run time to ensure all zones were exposed to a similar volume of fine sediment.

[16] Surface and subsurface sediment samples were taken for grain-size analysis following the termination of each run. Six sediment cores were sampled in each zone for all experiments. Sediment cores were taken at the same locations for each run, and areas near zone boundaries were not sampled. Sediment cores were sampled using a 12-cm-diameter, thin-gage sheet metal tube cut with triangular teeth at the bottom (similar in design to a McNeil bed sampler) which was driven into the bed. The surface layer was sampled prior to driving the sampler into the bed. The sampling thickness of the surface layer ranged from 1 to 3 cm depending on the grain-size distribution of the surface material for a given zone, or roughly two median diameters of the bed material. The metal sampler was driven into the subsurface after the surface layer was removed, and sediment inside the sampler was removed, typically in 2 to 5 layers through the remaining experimental sediment deposit. The thickness of each layer and the number of layers at each location were determined by the sampling technician

Table 2. Parameters for the Three Experimental Runs

	Initial Bed Slope	Water Discharge (l/s)	Bed Material Feed Rate	Fine Sediment Feed Rate, kg/min	Duration of Fine Sediment Feed, hours	Additional Run Time Following Termination of Fine Sediment Feed, hours
Run 1	0.004	40	none	0.209	100	0
Run 2				2.09	10	3.0
Run 3				20.9	1	2.5

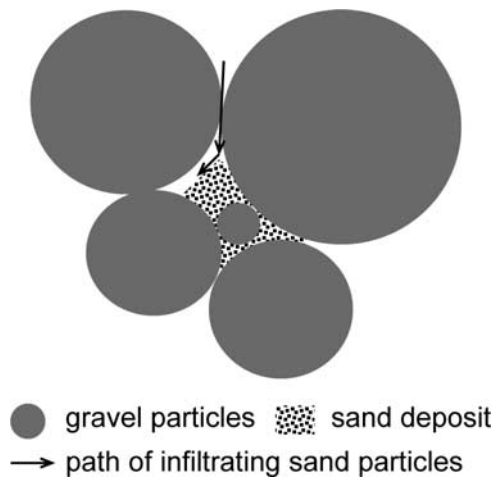


Figure 3. A schematic sketch of sand infiltration into gravel bed material as observed through the glass sidewalls of the flume. Sand deposits are resting at the angle of repose within pore spaces formed in the gravel interstices, demonstrating that sand infiltration was driven primarily by gravity.

based on visual observations of variations in sand content in the deposit using the following guidelines: (a) each layer must have a minimum 2-cm thickness to allow for adequate sediment for grain-size analysis; and (b) a new layer should be started if visual observations indicate a vertical change in fine sediment content. To aid in determining the thickness of each subsurface layer, test cores and/or trenches were often excavated in the zones (sufficient distance away from pre-determined experimental core locations so disturbance would not occur) to view the stratigraphy of the fine sediment infiltration prior to excavating the experimental cores.

[17] Surface and subsurface samples were dried, sieved at 1/2-phi intervals and analyzed to obtain the FSF value and the grain-size distribution of the gravel portion of each sample. In addition, the fine sediment was sieved at 1/4-phi intervals for five of the zones (i.e., zones 1, 5, 6, 9, and 10) for all runs to determine if any longitudinal sorting of the fine sediment feed occurred. This analysis indicated that for both longitudinal location and sediment depth there was minimal variation in the grain-size distributions of the infiltrated fine sediment (e.g., variation in median diameter is less than 2%). Thus the analyses presented in this paper assume that the grain-size distribution of the infiltrated fine sediment throughout the experimental zones is identical to that of the fine sediment feed.

3. General Observations During the Experimental Runs

3.1. Run 1 (Sand Feed Rate = 0.209 kg/min for 100 h)

[18] The introduced sand transported downstream predominantly as bed load. Initially, sand was transported predominantly near the center of the flume, forming a transport belt approximately half of the flume width. Sand deposits formed as patches within the transport belt in the interstices of the surface gravel. The sand transport belt

gradually widened over time and eventually covered the full width of the flume throughout the flume length by the termination of the run. Bed forms did not develop during the run, and topographic scans during and after the run indicated that bed slope remained at 0.004 throughout the run. Observations of sand infiltration were made through the glass walls on both sides of the flume throughout the flume length. Sand particles were observed falling into the pore spaces of the gravel deposit near the glass walls as soon as sand transport reached the glass walls. Sand infiltration into the gravel interstices appeared to be driven by gravity, evidenced by observations of small sand piles resting at the angle of repose within gravel interstices during sand infiltration (demonstrated in the sketch shown in Figure 3). No lateral transport of sand particles in the subsurface was observed other than sliding downslope along the sand piles (Figure 3).

[19] A 100-h duration for Run 1 was not predetermined before the experiment. A decision to terminate the run was made during the experiment based on observations that sand infiltration had reached equilibrium at the two glass walls throughout the length of the flume. The width of active sand transport widened to the glass walls after covering the rest of the flume, which implies that sand infiltration near the glass walls received the shortest duration of sand influx available for infiltration. Thus we assumed that sand had stopped infiltrating the middle portions of the flume bed where sampling stations were located once sand infiltration along the two walls reached equilibrium.

3.2. Run 2 (Sand Feed Rate = 2.09 kg/min for 10 h)

[20] Similar to Run 1, sand transported downstream predominantly as bed load and started in a sand transport belt near the center of the flume, which gradually widened to cover the full flume width before the termination of sediment feed. Figure 4 illustrates the sediment deposit at 4 h 15 min, indicating that the sediment deposition had not yet reached the left glass wall. With an increase in sand feed rate by a factor of 10, Run 2 produced more surface sand deposition than Run 1. At the end of the 10-h sand feed, the flume slope had increased to close to 0.005 from the initial slope of 0.004. Thicker sand deposition was measured along the flume centerline than near the flume walls. The sand deposit thickness averaged along the channel centerline was approximately 2 cm, and the sand deposit thickness averaged across the entire channel width was approximately 1 cm. Following termination of the sand feed, an additional 3 h of discharge without sediment feed transported the sand pulse to the flume exit, cleaning the bed surface prior to bed material sampling. Topographic scans at experiment termination indicated that the channel had returned to its initial bed slope of 0.004, except for Zone 9 (finest bed material distribution) where significant erosion occurred during the run. Because of this bed scour, data from Zone 9 for Run 2 are excluded in analyses presented below.

3.3. Run 3 (Sand Feed Rate = 20.9 kg/min for 1 h)

[21] The increased sand feed rate greatly exceeded the transport capacity of the experimental set-up and a large sand wedge formed in the upper half of the flume. At the end of the 1-h sand feed, the average sand deposit thicknesses in the upstream and downstream halves of the flume were 6 cm and 2.5 cm, respectively. As a result, the bed



Figure 4. Photograph of the sand deposit prograding downstream over the gravel bedded channel for Run 2 at 4 h 15 min run time. Photograph is looking downstream. Note that the sand deposit has not covered the bed along the left wall in this picture.

slope increased to approximately 0.006 from the initial slope of 0.004. Sand dunes (amplitude 2.0 cm, wavelength 40 cm) were observed throughout the flume. Where the local slope was steepest, upper flow-regime bed forms were observed as periodic antidunes and surface flow waves formed and dissipated. Following sand feed termination, flow without sediment feed continued for 2.5 h, which transported the sediment pulse out of the flume and cleaned the bed surface prior to bed material sampling. Bed scans at the termination of the run indicated that the bed returned to the initial slope of 0.004.

4. Overview of Experimental Analysis

[22] In the analyses presented below, we derive relations delineating the FSF in the gravel deposit as a result of fine sediment infiltration. Because of the complexity of the physical processes and the many parameters involved in the relations derived below, the analyses are broken into smaller components based on physical principles, and each component is presented separately. The results from the individual components are then combined to obtain the final

relations. For example, the saturated FSF (i.e., the maximum possible FSF in a frame-supported sediment deposit) is derived by breaking the problem into: (a) the pore space available in the clean gravel deposit; and (b) how much fine sediment can fit into the available pore space. Because all the numerical analyses presented below are sequential, with the subsequent equations depending largely on previous analyses, we encourage readers interested in the derivations of the numerical relations to read sequentially through all the related analyses sections.

5. Derivation of Saturated FSF Relation From Run 1 Data

[23] A frame-supported sediment deposit typically describes a deposit where the larger, supporting particles (gravel in these experiments) are in contact with each other while the smaller “matrix” material (fine sand in these experiments) fills the pores formed by the large particles. To facilitate description and analyses of the experimental results, we introduce the concept of a saturated FSF to quantify the maximum possible FSF in a frame-supported sediment deposit as described above. Once the FSF within a deposit exceeds the saturated FSF, the deposit no longer is fully frame-supported (i.e., becomes partially frame- and matrix-supported or matrix-supported, where coarser sediment particles are not necessarily in contact with one another), which usually occurs as a result of concurrent deposition of both coarse and fine sediment during bed mobilizing flow events.

[24] For deriving relations presented in this paper, we assume that the saturated FSF value of a sediment deposit is a function of the grain-size distributions of the coarse (framework bed material) and infiltrating fine sediment (sediment <2 mm throughout this paper). For fine sediment infiltration into an immobile gravel deposit initially void of any fine sediment, the pore space of the gravel deposit available for fine sediment infiltration is a function of the grain-size distribution and particle shape of the gravel deposit, and the grain-size distribution and particle shape of the fine sediment will determine how much fine sediment will be able to fit into the pore space of the gravel deposit. In the analyses presented hereafter, we neglect the influence of particle shape in determining pore space and the amount of fine sediment infiltration.

[25] To quantify the pore space available within a clean gravel deposit for fine sediment infiltration and the porosity of the fine sediment itself once deposited within the gravel pores, we measured porosities and grain-size distributions of 35 unimodal samples mixed from sediment ranging in diameter from 0.075 mm to 22 mm. Samples were mixed with unimodal distributions so that they were geometrically similar to fine sediment deposits when scaled down or to gravel deposits void of fine sediment when scaled up. Both the sediment samples used for porosity testing and the bed material in the flume during sediment infiltration runs were lightly packed by hand. Thus the calculated porosity to geometric standard deviation relationship is expected to characterize the flume sediments well, but the relationship’s applicability to naturally, fluvially packed sediments is unknown. Porosities for the 35 samples were measured using a direct water saturation method [Bear, 1972] in a 1-liter container. Following porosity measurements, samples

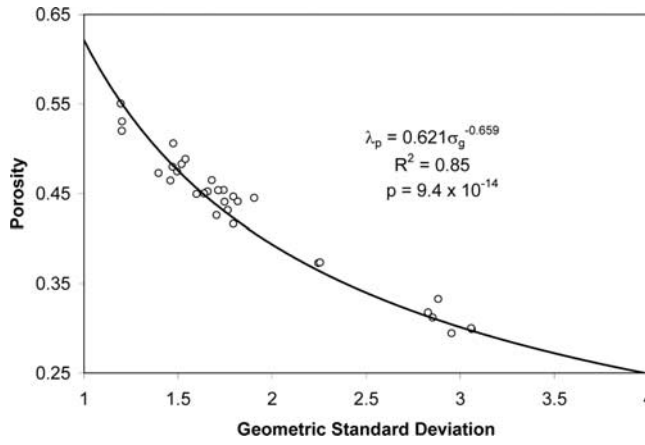


Figure 5. Measured porosity of unimodal sediment mixtures as a function of their geometric standard deviations.

were sieved and analyzed for grain-size distributions to obtain their geometric standard deviations.

[26] The porosity of the 35 samples ranged between 0.25 and 0.55, and the geometric standard deviation ranged between 1.20 and 3.06. The range of above porosity values is approximately the same as those provided by *Allen* [1985], who reported porosity values of 0.297 to 0.554 for loosely and densely packed sand, glass beads, long-grain rice and chopped spaghetti. Measured porosities were then correlated with the geometric standard deviations of the samples (Figure 5). Three outliers were removed from the 35 samples because they obviously deviated from the porosity to geometric standard deviation relationship from the other samples and are attributed to measurement error during porosity and/or grain-size analysis.

[27] A sediment deposit with relatively uniform sediment sizes (i.e., a small geometric standard deviation) will have greater porosity than one with a relatively wider range of sediment particle sizes (i.e., a large geometric standard deviation) [Allen, 1985]. Where a sediment deposit is composed of completely uniform particles (i.e., a geometric standard deviation of 1) a maximum porosity will be achieved, and for a sediment deposit with a unimodal grain-size distribution composed of particles ranging from extremely large sizes to infinitely small ones (i.e., a geometric standard deviation approaching infinity) the available pore space should approach zero. Under these hypothetical limits, a function in the form of $\lambda_p = \alpha_1 \sigma_g^{-\beta_1}$ will provide one plausible description of the relation between porosity and geometric standard deviation of a unimodal sediment deposit, in which λ_p denotes the porosity of the deposit, σ_g denotes the geometric standard deviation of the deposit, and α_1 and β_1 are constant coefficients. Applying a least squares error regression to the experimental porosity data (shown in Figure 5) with the above relation resulted in $\alpha_1 = 0.621$ and $\beta_1 = 0.659$, or

$$\lambda_p = 0.621 \sigma_g^{-0.659} \quad (1)$$

Equation (1) is shown in Figure 5 as a solid line. We reiterate that equation (1) was derived based on porosity and

grain-size distribution measurements from 32 samples of unimodal sediment packed by hand, and the applicability of equation (1) to naturally packed sediment deposits or deposits with a bimodal distribution, a condition commonly found in natural sediment deposits in gravel-bedded rivers [e.g., *Parker*, 1990], is unknown.

[28] After establishing a relation between porosity and geometric standard deviation of a unimodal sediment deposit in equation (1), we then applied this relation to derive a semi-empirical relation for saturated FSF below.

[29] In a hypothetical case where the sand grain size is much smaller than gravel particles (i.e., $D_g/D_s \rightarrow \infty$, where D_g denotes the characteristic particle size of gravel and D_s denotes the characteristic particle size of sand), all the pore space in the gravel deposit can be filled with fine sediment particles and the pore space within the fine sediment. The solid volume and pore space available in the gravel deposit is calculated with $V_g = (1 - \lambda_g)V_t$ and $V_{gp} = \lambda_g V_t$, respectively, where V_g denotes the solid volume of gravel, V_{gp} denotes the volume of pore space left within the gravel deposit, and V_t denotes the total volume of the gravel deposit (i.e., the combined volume of solid and pores), and λ_g is porosity of the coarse sediment. Once the pore space within the gravel deposit is completely filled in with fine sediment under the assumption that $D_g/D_s \rightarrow \infty$, the volume of fine sediment (solid only) will be $V_s = (1 - \lambda_s)\lambda_g V_t$, where λ_s is porosity of the fine sediment, from which we obtain an expression for saturated FSF: $f_s = V_s / (V_g + V_s)$, or

$$f_s = \frac{(1 - \lambda_s)\lambda_g V_t}{(1 - \lambda_g)V_t + (1 - \lambda_s)\lambda_g V_t} = \frac{(1 - \lambda_s)\lambda_g}{1 - \lambda_s \lambda_g} \quad (2)$$

where f_s denotes the saturated FSF value for the deposit under the assumption that $D_g/D_s \rightarrow \infty$. The amount of fine sediment that can fit into the pores of a gravel deposit should decrease with an increase in fine sediment particle size because larger fine sediment particles are more difficult to fit into the gravel interstices, and thus, a more generalized expression of equation (2) is

$$f_s = \frac{(1 - \lambda_s)\lambda_g}{1 - \lambda_s \lambda_g} f_n(D_g/D_s) \quad (3a)$$

where $f_n(D_g/D_s)$ is a function of D_g/D_s . Substituting equation (1) into (3a) yields the following relation:

$$f_s = \frac{0.621 \left(1 - 0.621 \sigma_{sg}^{-0.659}\right) \sigma_{gg}^{-0.659}}{1 - 0.621^2 \left(\sigma_{gg} \sigma_{sg}\right)^{-0.659}} f_n(D_g/D_s) \quad (3b)$$

where σ_{sg} denotes geometric standard deviation of the infiltrating fine sediment and σ_{gg} denotes geometric standard deviation of the gravel deposit that the fine sediment infiltrates.

[30] As discussed earlier, the saturated FSF is at its maximum value of $(1 - \lambda_s) \lambda_s / (1 - \lambda_s \lambda_g)$ when $D_g/D_s \rightarrow \infty$, and decreasing D_g/D_s will result in a decrease in the saturated FSF value. That is, the function $f_n(D_g/D_s)$ must satisfy (a) $f_n(\infty) = 1$, and (b) $f_n(D_g/D_s)$ increases monotonically with an increasing D_g/D_s . A simple exponential

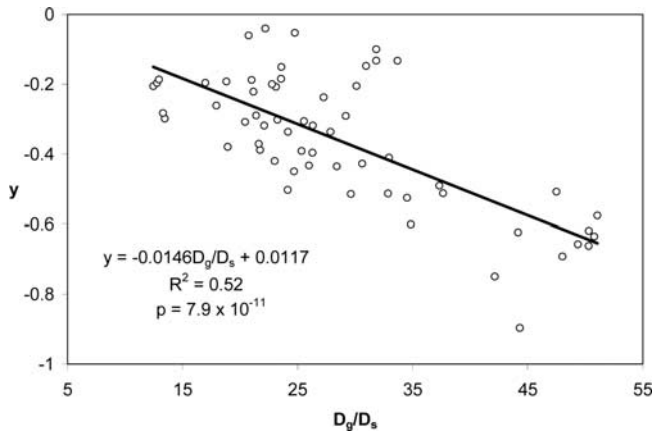


Figure 6. Linear regression with Run 1 data from the top subsurface layer (i.e., subsurface immediately beneath the surface layer) to obtain relation between parameter y (defined in equation (5c)) and D_g/D_s .

function below (equation (4)) satisfies both conditions (a) and (b), and is used for subsequent analyses:

$$f_n(D_g/D_s) = 1 - \exp(-\alpha_2 D_g/D_s + \beta_2) \quad (4)$$

where α_2 and β_2 are coefficients determined with experimental data. Note that, formulations other than equation (4) may also be used for this analysis as long as they are smooth and satisfy the two conditions specified above.

[31] Using the geometric mean grain sizes of the coarse sediment (D_{gg}) and fine sediment (D_{sg}) as representative grain sizes, and substituting equation (4) into (3b), we obtain:

$$y = -\alpha_2 x + \beta_2 \quad (5a)$$

where

$$x = \frac{D_{gg}}{D_{sg}}, \quad (5b)$$

and

$$y = \ln \left(1 - \frac{[1 - 0.621^2 (\sigma_{gg} \sigma_{sg})^{-0.659}] f_s}{0.621 (1 - 0.621 \sigma_{sg}^{-0.659}) \sigma_{gg}^{-0.659}} \right) \quad (5c)$$

Following equation (5a), coefficients α_2 and β_2 in equation (4) can be obtained through a simple linear regression using paired (x , y) data calculated with equations (5b) and (5c).

[32] As discussed earlier, sand infiltration was deemed to have ceased by the termination of Run 1. Thus we consider the sand content in the top subsurface layer for that run as approximating the saturated FSF. Note that the thickness of this top subsurface layer ranges between approximately 2 cm to 10.5 cm, depending on the varying FSF values found within different bed material zones. Using data from the top

subsurface layer from Run 1 for a linear regression with equation (5a), the two regression coefficients obtained are $\alpha_2 = 0.0146$ and $\beta_2 = 0.0117$ (shown in Figure 6). Substituting the two coefficients back into equations (4) and (3b) yields the following relation:

$$f_s = \frac{0.621 (1 - 0.621 \sigma_{sg}^{-0.659}) \sigma_{gg}^{-0.659}}{1 - 0.621^2 (\sigma_{gg} \sigma_{sg})^{-0.659}} \cdot \left[1 - \exp \left(-0.0146 \frac{D_{gg}}{D_{sg}} + 0.0117 \right) \right] \quad (6)$$

A comparison of equation (6) with Run 1's top subsurface data (i.e., the data used to derive the constant coefficients in equation (6)) is shown in Figure 7. The relatively good agreement between the measured sand fraction and predicted saturated FSF values indicates that the general physical principles applied in formulating equation (6) are reasonable. Comparison of equation (6) with data from Runs 2 and 3 and fine sediment infiltration at a depth beyond the top subsurface layer is presented and discussed in the next two sections.

[33] Note a two-step sequential regression procedure was used to derive equation (6), in which the second-step analysis is dependent on the result of the first-step. In a multiple-step sequential regression analysis, a later step analysis does not augment errors carried over from the early steps. On the contrary, a later step regression provides an opportunity to correct errors, including potential human operational mistakes, introduced in the early steps, potentially reducing the errors from the early steps.

6. Comparison of Runs 2 and 3 With the Saturated FSF Relation

[34] The FSF values from the top subsurface layers for Runs 2 and 3 are presented in Figure 8, where the ordinate axis represents saturated FSF values predicted with equation (6) based on the measured local gravel grain-size distribution and the grain-size distribution of the infiltrating fine sediment, and the abscissa axis is the measured saturated FSF. Figure 8 indicates that Run 2 data are more or less

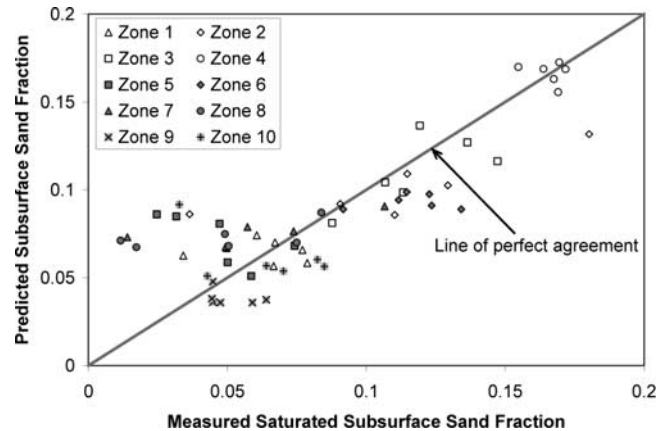


Figure 7. Comparison of equation (6) predictions with experimental data from the top subsurface layer (i.e., subsurface immediately beneath the surface layer) in Run 1.

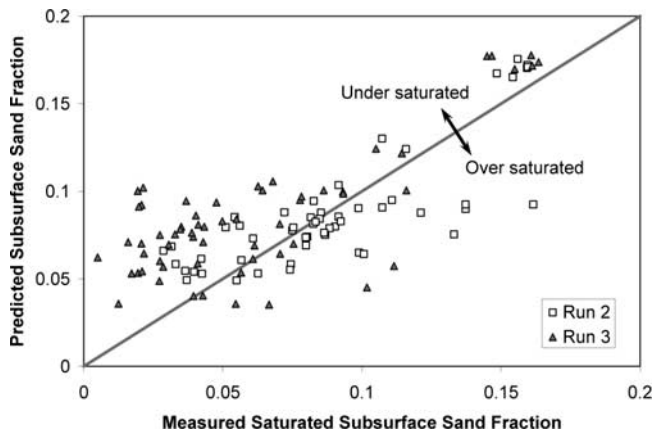


Figure 8. Comparison of equation (6) predictions with experimental data from the top subsurface layer (i.e., subsurface immediately beneath surface layer) in Runs 2 and 3.

evenly distributed around the solid line (line of perfect agreement between measured and predicted) but have more scatter than the measured versus predicted for Run 1 data (Figure 7). However, the data from Run 3 are primarily located above the solid line (i.e., predicted saturated FSF is higher than the measured value), indicating that Run 3 resulted in less fine sediment infiltration to the top subsurface layer than Runs 1 and 2. If the assumption that the top subsurface layer of Run 1 approximated saturation with fine sediment is valid, then Run 2’s top subsurface layer appears to be similarly saturated with fine sediment while the top subsurface layer in Run 3 is mostly under saturated with fine sediment. Comparing the average FSF in the top subsurface layer for all zones in each run also shows less fine sediment infiltrated during Run 3 (Figure 9). Because Runs 2 and 3 had fine sediment feed rates 10 times and 100 times of that of Run 1, respectively, we conclude that fine sediment infiltration to the top subsurface layer decreases once the fine sediment feed rate increases beyond a certain threshold. We believe this is a reasonable conclusion for an immobile bed, because once the fine sediment supply exceeds the transport capacity, fine sediment will bury the bed surface, which will limit additional fine sediment particles from infiltrating the gravel pores.

7. FSF Throughout the Vertical Subsurface Column and Derivation of Vertical FSF Profile

[35] FSF values by weight for all the subsurface layers sampled (i.e., the entire subsurface vertical column) are presented by zone for the three runs in Figure 10 (the solid lines in Figure 10 are from an empirical relation derived below). Two primary data trends are evident from the diagrams in Figure 10: (a) FSF values for Run 3 are generally lower than that for Runs 1 and 2, supporting the results shown in Figures 8 and 9; and (b) FSF values generally decrease with depth into the bed. Comparing the FSF values in Zones 1 and 10 (the two zones with identical bed material grain-size distributions) indicates that there may have been slightly more fine sediment infiltration in Zone 10 (the downstream-most zone) than Zone 1

(Figures 10a and 10j). A closer comparison of the two zones for each individual run, however, indicated that the higher sand fraction for Zone 10 occurred only during Run 1, while there is no clear pattern for data from the other two runs. Given that, the comparison between Zones 1 and 10 is inconclusive.

[36] Based on the experimental results presented in Figure 10, we determined that an exponential decay function adequately approximate the vertical profile of infiltrated FSF in our experiments. Thus we use our experimental data to fit an exponential decay function to derive a semi-empirical relation that describes the vertical FSF profile when fine sediment infiltrates a clean gravel deposit. Applying an exponential decay function is supported by Cui *et al.* [2008], who derived a theory based entirely on physical principles. On the basis of this theory, an exponential decay function in depth can characterize the amount of fine sediment infiltration into an initially clean gravel deposit if the fine sediment trapping coefficient (defined as the fraction of fine sediment trapped in the deposit as it infiltrates a unit distance) is independent of the FSF in the deposit. Cui *et al.* [2008] also showed that an exponential decay function can approximate the vertical FSF profile if fine sediment trapping coefficient is weakly dependent on FSF value of the deposit. Although an exponential decay function will not allow the sand fraction values to reach zero, for practical purposes, a reasonably low sand fraction (i.e., ≤ 0.01) can usually be considered as negligible.

[37] To further simplify the analysis, we assume that sand content reaches saturation at a depth twice the gravel geometric mean size. This assumption is primarily based on our experimental set-up where the subsurface begins at a depth approximately twice the geometric mean bed material grain size. This implies that flow can flush fine sediment to a depth of approximately twice the gravel geometric mean grain size without mobilizing the gravel particles. Implementing this assumption into an exponential decay function, the FSF as a function of depth can be expressed as:

$$\frac{f}{f_s} = \exp \left[-\beta \left(\frac{z}{D_{gg}} - 2 \right) \right] \tag{7}$$

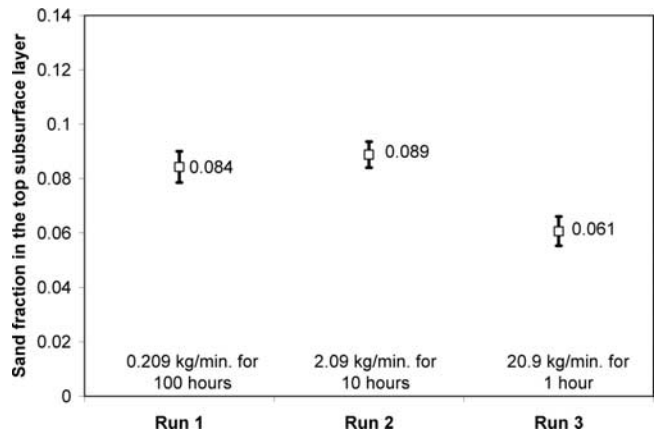


Figure 9. Average sand fraction \pm standard error (error bars) in the top subsurface layer of all zones, providing a simplified comparison of fine sediment infiltration for the three runs.

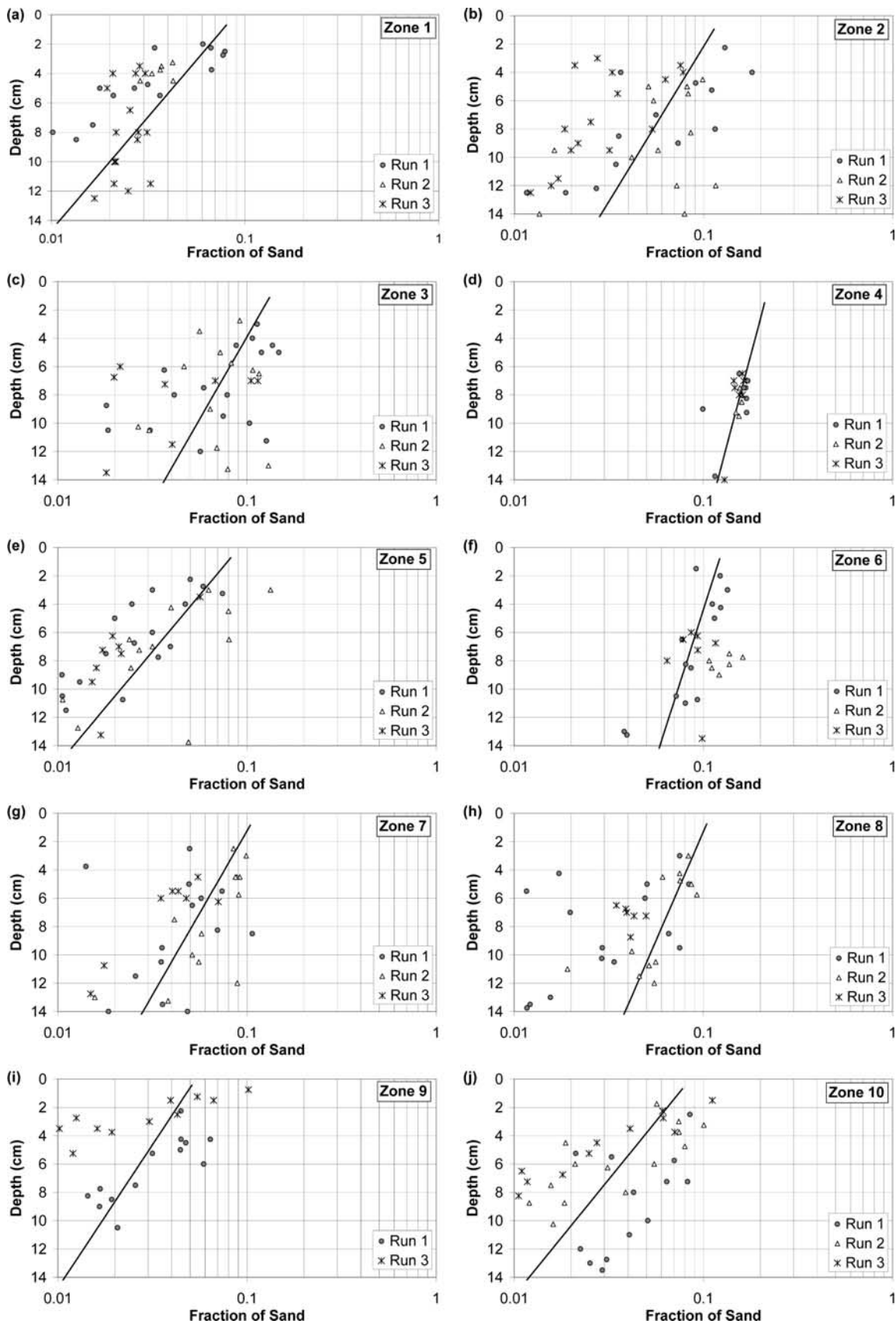


Figure 10. Comparison of the subsurface sand fraction (by weight) for the three runs in each of the ten zones. The solid line in each diagram is the predicted equilibrium vertical fine sediment fraction profile with equations (6) and (12). Data for Run 2 in Zone 9 are not presented due to channel degradation within that zone during the experiment.

Table 3. β Values Obtained for the Ten Zones Using Data From Runs 1 and 2 and Parameters Averaged by Zone for Regression Analyses Used to Calculate the Vertical FSF Profile Relation

Zone	1	2	3	4	5	6	7	8	9	10
β	0.1892	0.1030	0.1025	0.0880	0.1281	0.0244	0.0748	0.1035	0.0405	0.0807
$D_{gg}\sigma_{gg}/D_{sg}^a$	42.93	51.74	61.08	62.84	43.25	33.70	44.07	35.61	23.55	39.68
σ_{gg}^a	1.89	1.71	1.71	1.32	1.87	1.33	1.65	1.48	1.73	1.84

^aParameters are averaged over all samples within each zone.

in which f denotes the FSF; z denotes the depth into the deposit measured from the surface of the coarse sediment deposit, and the exponential coefficient β is a function of coarse to fine characteristic grain-size ratio (i.e., D_g/D_s). On the basis of the theories developed in Cui *et al.* [2008], β/D_{gg} is the trapping coefficient for the infiltrating fine sediment with a unit of $[\text{Length}]^{-1}$.

[38] We used data from Runs 1 and 2 to determine a semi-empirical relation describing the vertical FSF profile in the form of equation (7); data from Run 3 are excluded because the run resulted in mostly under-saturated FSF values in the top subsurface layer as shown in Figure 8. To derive the semi-empirical relation, we separated the analysis into two steps. In the first step we expect that the β values for all the samples within a specific zone should be very similar and subsequently assume that there is one β value for each individual zone (a total of 10 β values can be obtained from the 10 zones). The β value for each zone was obtained through a least squares error regression from data for all sample cores from Runs 1 and 2, assuming a relation in the form of equation (7) and using equation (6) to calculate f_s . In this analysis, the D_{gg} value for each zone was taken as its target value presented in Table 1 for simplicity. β values obtained for the 10 zones are presented in Table 3.

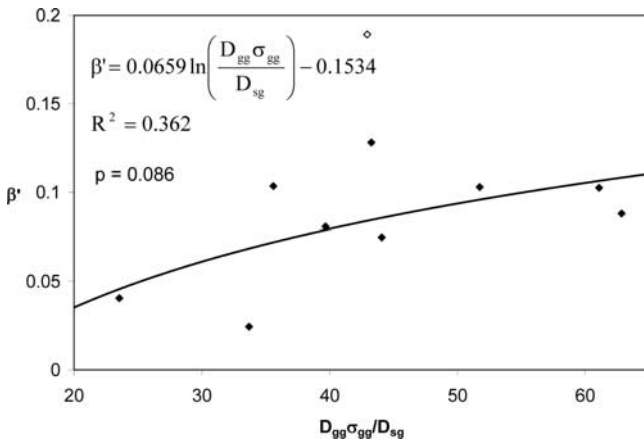


Figure 11. Parameter β' (β' is used to indicate an intermediate formulation for β which differs from the final equation for β) and $D_{gg}\sigma_{gg}/D_{sg}$ values for the 10 zones derived from Runs 1 and 2 data. The regression (solid line) is derived assuming that β is independent of other sediment grain size parameters. One data point (open diamond) was arbitrarily excluded as an outlier from the regression equation based on visual determination. Inclusion of the outlier produced negligible changes to the final results of the vertical fine sediment fraction profile.

[39] Once β values were determined for each zone, we developed a relation that correlates β values to the grain-size distributions of the coarse and fine sediments. We assume that the exponential coefficient β is a function of the gravel geometric standard deviation (σ_{gg}), which determines the pore space available in the gravel deposit, and the coarse to fine characteristic grain-size ratio (D_g/D_s), which describes the size of the pore opening relative to the infiltrating fine sediment grain size. The geometric mean grain size (D_{sg}) was chosen as the characteristics grain size for fine sediment due to its relatively uniform grain-size distribution for our experiments. Two characteristic grain sizes for gravel were initially tested for the analysis: D_{gg} (geometric mean grain size) and $D_{gg}\sigma_{gg}$ (equivalent to the D_{84} if the grain-size is log-normally distributed). For our experimental data, we found that both metrics of characteristic gravel grain size produced very similar results. In the analyses presented hereafter, $D_{gg}\sigma_{gg}$ is used as the representative gravel grain size.

[40] In order to correlate β values with parameters σ_{gg} and $D_{gg}\sigma_{gg}/D_{sg}$, both of these parameters were averaged for all the samples within each zone (averaged values are presented in Table 3). We separated the second step into two sub-steps to simplify the regression process, where the first sub-step seeks a $\beta \sim D_{gg}\sigma_{gg}/D_{sg}$ relation independent of σ_{gg} , and the second sub-step introduces parameter σ_{gg} through an additional correlation.

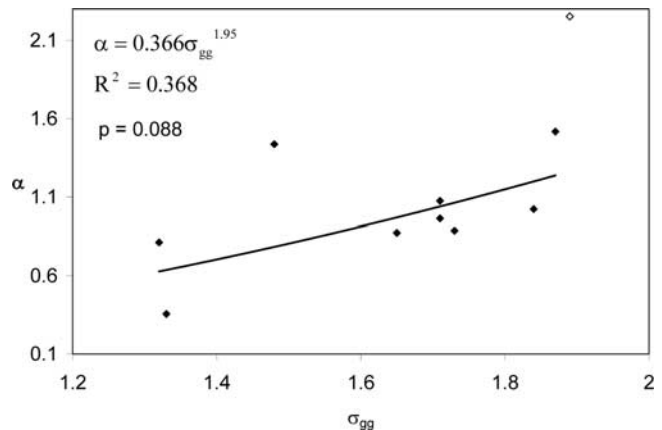


Figure 12. Parameter α (as defined in equation (10b)) plotted against σ_{gg} values for the 10 zones and a regression between the two parameters assuming a power relation. The one outlier excluded from the regression analysis shown in Figure 11 is excluded in this regression for consistency.

[41] The $\beta \sim D_{gg}\sigma_{gg}/D_{sg}$ relation based on data in Table 3 is shown in Figure 11, and the resultant regression equation for β by assuming that β is independent of σ_{gg} is:

$$\beta' = 0.0638 \ln\left(\frac{D_{gg}\sigma_{gg}}{D_{sg}}\right) - 0.149 \quad (8)$$

in which β' is an estimator for β when σ_{gg} is neglected. The correlation between β and σ_{gg} is introduced in the second sub-step by assuming that $\beta = \omega\beta'\sigma_{gg}^\gamma$ and then substituting equation (8) for β' :

$$\beta = \omega \left[0.0638 \ln\left(\frac{D_{gg}\sigma_{gg}}{D_{sg}}\right) - 0.149 \right] \sigma_{gg}^\gamma \quad (9)$$

where ω and γ are coefficients determined through regression accomplished by rearranging equation (9) as:

$$\alpha = \omega\sigma_{gg}^\gamma \quad (10a)$$

where

$$\alpha = \frac{\beta}{0.0638 \ln\left(\frac{D_{gg}\sigma_{gg}}{D_{sg}}\right) - 0.149} \quad (10b)$$

Coefficients ω and γ were obtained with a least squares error regression (shown in Figure 12) and were determined to be:

$$\omega = 0.366, \quad (11a)$$

$$\gamma = 1.95 \quad (11b)$$

Substituting equations (11a) and (11b) into equations (9) and (7) yields the following relation for the vertical FSF profile:

$$\frac{f}{f_s} = \exp\left\{-0.0233\sigma_{gg}^{1.95} \left[\ln\left(\frac{D_{gg}\sigma_{gg}}{D_{sg}}\right) - 2.44 \right] \left(\frac{z}{D_{gg}} - 2\right)\right\} \quad (12)$$

The vertical FSF profile calculated with equation (12) for each zone is shown in Figure 10 as a solid line. The regressions used to derive equation (12) shown in Figures 11 and 12 have low R^2 values, and comparisons of the predicted sediment fractions with experimental data shown in Figure 10 also exhibit a wide range of scatter between predicted and observed values. Limitations notwithstanding, equation (12) predictions capture the general magnitude and trend of FSF values at depth into the deposit and are considered reasonable first-order approximations for assessments.

8. Quantitative Assessment of the Semi-Empirical Relations

[42] Below we provide a quantitative performance assessment of the semi-empirical relations for calculating the saturated FSF (equation (6)) and the vertical FSF profile (equation 12) based on experimental data from all three

runs. In order to compare the experimental data across all runs and all ten bed material zones with the relations, we introduce the following non-dimensional (i.e., normalized) parameters:

$$\tilde{z} = 0.0233 \frac{\sigma_{gg}^{1.95}}{D_{gg}} \left[\ln\left(\frac{D_{gg}\sigma_{gg}}{D_{sg}}\right) - 2.44 \right] (z - 2D_{gg}) \quad (13)$$

$$\tilde{f} = \frac{f}{f_s} = \left\{ \frac{0.621 \left(1 - 0.621\sigma_{sg}^{-0.659}\right) \sigma_{gg}^{-0.659}}{1 - 0.621^2 \left(\sigma_{gg}\sigma_{sg}\right)^{-0.659}} \cdot \left[1 - \exp\left(-0.0146 \frac{D_{gg}}{D_{sg}} + 0.0117\right) \right] \right\}^{-1} f \quad (14)$$

where \tilde{z} is a non-dimensional depth as defined in (13), and \tilde{f} is the FSF normalized by the saturated FSF. By substituting equations (13) and (14) into (12), we obtain a dimensionless vertical FSF profile:

$$\tilde{f} = \exp(-\tilde{z}) \quad (15)$$

Because equation (15) is free of parameters that vary by zone, we can collapse the data from all the zones into a single diagram with the dimensionless variables given in equations (13) and (14) (Figure 13a). Figure 13a demonstrates that the experimental data have a large variance due to the stochastic nature of the physical processes of fine sediment infiltration. An informative quantitative performance metric of the semi-empirical relations cannot be calculated via a direct comparison between the model predictions and experimental data, because such a comparison would primarily characterize the variance of the experimental data rather than measure model performance.

[43] A more applicable performance metric for the relations was achieved by comparing model predictions with a series of moving-averages of the experimental data. We calculated 32 weighted-averaged values for \tilde{z} , ranging between 0.05 and 1.60 with 0.05 step increments. The weighted-averaged values for a given \tilde{z} value were calculated from equation (16) below:

$$\tilde{f}_* = \frac{\sum(w_i \tilde{f}_i)}{\sum w_i} \quad (16)$$

where \tilde{f}_* denotes the weighted-averaged \tilde{f} value at \tilde{z} ; \tilde{f}_i denotes the i -th flume measurement of the \tilde{f} value, and w_i is the weighting factor associated with the i -th measurement at \tilde{z} calculated from equation (17):

$$w_i = \exp(-k|\tilde{z} - \tilde{z}_i|) \quad (17)$$

where k is an exponential coefficient; \tilde{z} is the coordinate where the weighted-averaged \tilde{f} value is calculated, and \tilde{z}_i denotes the \tilde{z} value of the i -th measurement. For assessing our experimental data we used $k = 30$, which resulted in the weighting function (equation (17)) shown in Figure 13b. Figure 13a indicates that equation (15) closely matches the weighted-averaged \tilde{f} values from the measured data.

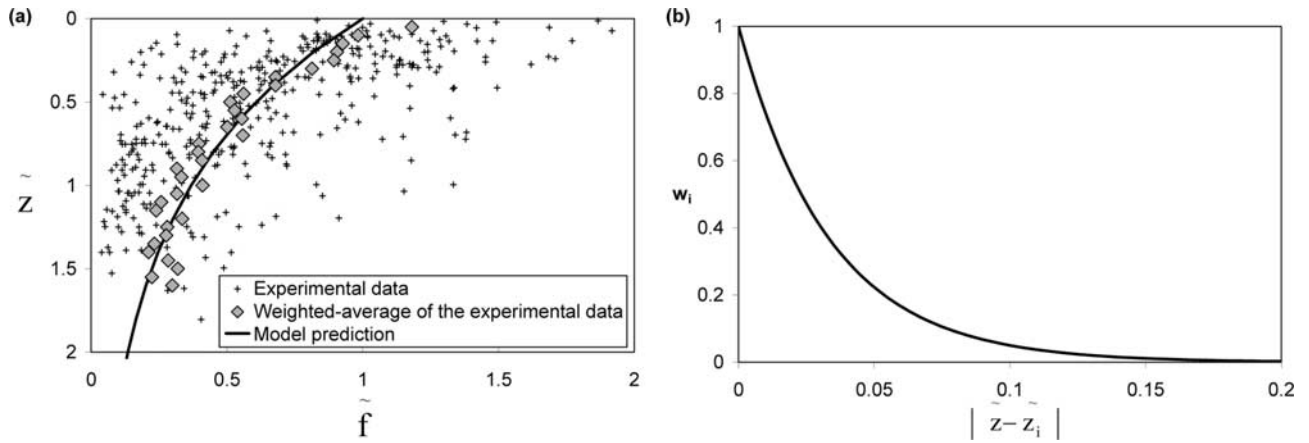


Figure 13. (a) Comparison of model predictions with experimental data. (b) Weighting factor used for calculating the weighted-averaged dimensionless fine sediment fraction shown in Figure 13a.

Increasing or decreasing the exponential coefficient k value will result in an increase or a decrease, respectively, in the variance of the weighted-averaged \tilde{f} values, but does not significantly change the observation that the weighted-averaged \tilde{f} values closely match the predicted values from the numerical relations.

[44] A root mean square error (RMSE) between numerical relation predictions and weighted-averaged experimental data was calculated to characterize model performance according to equation (18):

$$\varepsilon = \sqrt{\frac{1}{N} \sum (\tilde{f}_{pi} - \tilde{f}_{*i})^2} \quad (18)$$

where ε denotes RMSE between model prediction and weighted-averaged data; N denotes the number of samples ($N = 32$ in our case); \tilde{f}_{pi} denotes the i -th predicted \tilde{f} value; and \tilde{f}_{*i} denotes the i -th weighted-averaged \tilde{f} value. The ε value calculated with equation (18) based on the data shown in Figure 13a is 0.073. Because \tilde{f} is the FSF value (f) normalized with the saturated FSF value (f_s), the RMSE between model prediction and the weighted-averaged FSF

value is 7.3% of the saturated FSF value, reflecting a reasonable agreement between predicted and the weighted-averaged experimental data. The reasonable agreement between predicted and weighted-averaged experimental data was expected because equation (12) was formulated as an exponential decay function with depth, which is consistent with the theoretical derivations for fine sediment infiltration by *Cui et al.* [2008].

9. Depth of Fine Sediment Infiltration

[45] To better understand the depth that fine sediment infiltrates into a gravel deposit, equation (12) was rearranged to calculate $z/D_{gg} \sim D_{gg}\sigma_{gg}/D_{sg}$ relations for three

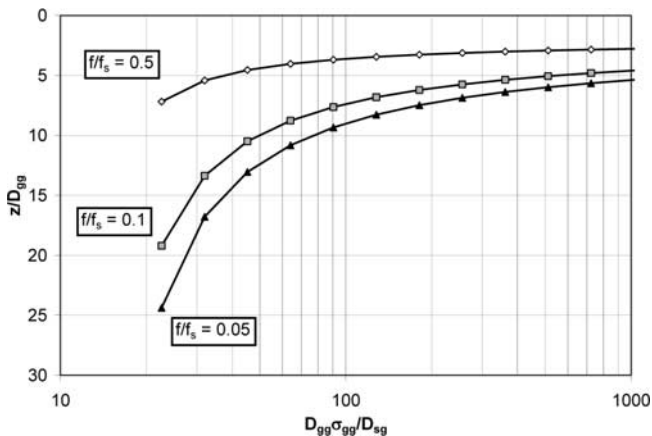


Figure 14. Predicted depths (z) relative to the gravel geometric mean grain size (D_{gg}), where the fine sediment fraction reaches 50% (i.e., $f/f_s = 0.5$), 10%, and 5% of the saturated FSF value. The gravel geometric standard deviation (σ_{gg}) is assumed to be 3.0.



Figure 15. Photograph of the sediment deposit from Zone 5 at the termination of Run 1, illustrating the limited fine sediment infiltration depth. Ruler scales are inches (left) and centimeters (right).

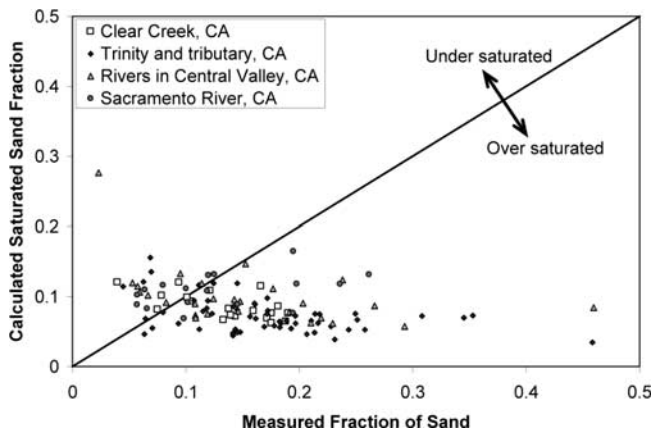


Figure 16. Field measurements of fine sediment fractions in select rivers in California (CA) compared to the saturated fine sediment fraction calculated with equation (6). Field data are provided by Matt Brown and Jess Newton of the USFWS for Clear Creek, CA; *Graham Matthews and Associates* [2003, 2004] for the Trinity River and tributaries; and *CDWR* [1994, 1995] for the Sacramento River and other rivers in the Central Valley, CA.

f/f_s values (0.5, 0.1, and 0.05, which represent the depth relative to mean bed material size where the sand fraction reduces to 50%, 10%, and 5% of the saturated FSF value, respectively). For the example curves presented in Figure 14, we assume $\sigma_{gg} = 3$, a typical value for gravel deposits (that exclude <2 mm particles) in natural rivers. On the basis of more than one hundred grain-size distributions sampled from gravel bedded rivers in Alberta, Canada by *Shaw and Kellerhals* [1982], $D_{gg}\sigma_{gg}/D_{sg}$ values in gravel bedded rivers are typically on the order of 50 or greater. On the basis of the curves illustrated in Figure 14, we can expect that FSF values decrease to 50%, 10%, and 5% of the saturated FSF value at depths of approximately 4, 9, and 11 times the gravel geometric mean size, respectively. Results in Figure 14 and observations from our sample cores and trenches in the flume experiments (see Figure 15) illustrate the rapid decrease in fine sediment content with depth into the deposit.

10. Discussion

[46] Direct comparison of the results from the three experimental runs indicates that a higher magnitude supply rate of fine sediment produces similar or less fine sediment infiltration into a static gravel bed than slower more prolonged delivery rates of equivalent volumes of fine sediment. This observation can have important ramifications for dam-removal projects, where one objective is often to minimize fine sediment infiltration, and suggests that staged dam removals that control and prolong the duration of fine sediment delivery to reaches downstream of the dam will likely produce as much if not more fine sediment infiltration than a rapid one-stage dam removal. However, accelerated releases of fine sediment will likely result in temporarily thicker fine sediment surface deposits as observed in our Run 3 and demonstrated numerically in *Cui et al.* [2006], which can have deleterious ecological impacts.

[47] The relations for fine sediment infiltration presented in this paper are derived from experimental data that characterize the infiltration of fine sediment into clean gravel. In natural rivers, however, even the cleanest gravel deposits contain at least a small fraction of fine sediment (Figure 16). Figure 16 compares field data collected from several rivers in California with the saturated FSF values calculated with equation (6). Data from Clear Creek, California are also depicted in Figure 17, which shows the longitudinal variation of fine sediment saturation along the river. Figures 16 and 17 indicate that the FSF values in most of the samples are higher than the saturated FSF values calculated with equation (6), which suggests that the sediment deposit is likely at least partially matrix-supported. The over-saturation of fine sediment is likely the result of concurrent deposition of coarse and fine sediment during bed aggradation rather than fine sediment infiltration [*Cui*, 2007a, 2007b]. This implies that during intermediate flow events where there is fine sediment transport without bed mobility, minimal or no additional fine sediment will be able to infiltrate most of the bed material samples shown in Figure 16 if the grain-size distribution of the potential infiltrating fine sediment supply is similar or coarser than that of the fine sediment already filling the pore spaces in the bed material. However, a sediment supply finer than the fine sediment occupying the bed material pore spaces may still infiltrate by filling in the pore spaces within the fine sediment residing in the bed material, resulting in an increase in the FSF.

[48] Observations and relations derived from our experimental data provide useful analogies for assessing cases where even finer sediment (e.g., silt or clay) could infiltrate a gravel-bed already saturated or oversaturated with sand. In order to discuss these analogies, it is useful to consider the physical processes controlling why the FSF value decreases with depth into the gravel deposit as a result of fine sediment infiltrating a gravel deposit initially void of fine sediment. We invoke the proposed hypothetical processes

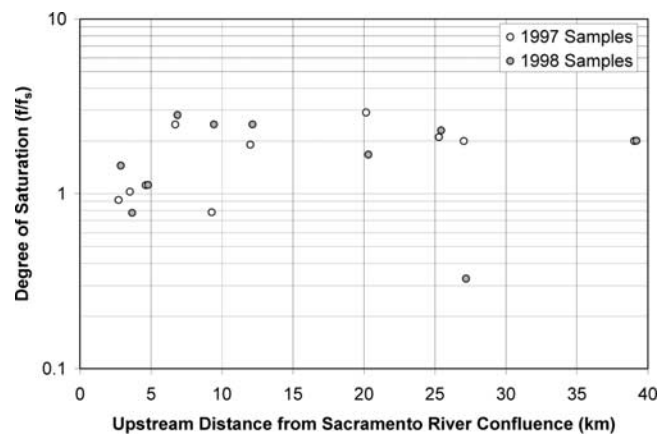


Figure 17. Degree of fine sediment saturation for Clear Creek in 1997 and 1998, based on field data provided by Matt Brown and Jess Newton of the USFWS. Saturated FSF values (f_s) are calculated with equation (6); $f/f_s > 1$ indicate over saturation relative to equation (6) predictions and $f/f_s < 1$ indicate under saturation relative to equation (6) predictions.

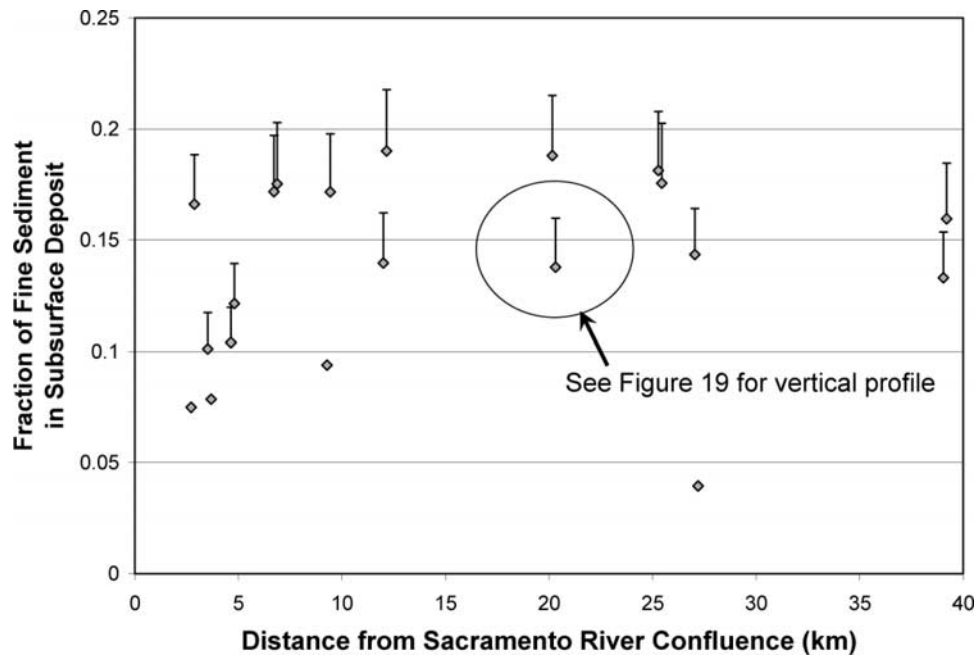


Figure 18. Subsurface sand fractions (diamonds) measured in Clear Creek, California. The vertical error bars depict the predicted (equations (6) and (12)) potential increase in the fine sediment fraction if silt with a geometric mean of 0.02 mm and a geometric standard deviation of 1.5 were to infiltrate the bed. Samples without error bars are currently under-saturated with sand and the potential infiltration of silt cannot be estimated with the relations presented in this paper. The large circle indicates the sample analyzed for the potential vertical fine sediment fraction profile, presented in Figure 19.

for fine sediment infiltration into a clean gravel deposit described by *Lauck* [1991] while developing his stochastic numerical model for fine sediment infiltration. *Lauck* [1991] proposed that once a fine sediment particle enters the pore space of a gravel deposit, it will either continue to travel downward within the pores or become lodged in place because it cannot pass through the geometry of the opening. Once lodged in place, a fine sediment particle becomes permanently locked in place (until mobilization of the bed material), which can reduce the size of the pore space opening and potentially increases the probability for subsequent infiltrating fine sediment particles to become lodged. This process results in a decreased FSF downward into the deposit. Eventually the top layer of the deposit will be completely clogged with fine sediment particles (i.e., bed material becomes saturated with fine sediment), which prevents fine sediment from passing through to the lower layers and effectively stops fine sediment infiltration deeper into the deposit. For cases of sand particles infiltrating a clean gravel bed (i.e., our flume experiments), the downward movement of the fine sand particles was driven by gravity. However, for cases of silt particles infiltrating a gravel bed already saturated with sand, the downward movement of silt particles could be driven by a combination of gravity and downward intra-gravel flow. Despite the differences in the driving forces for the downward movement of fine sediment particles, because particle lodging is a function of geometric fitting [*Lauck*, 1991], the mechanisms and processes affecting fine sediment particles clogging the pores of the deposit and forming a surface seal impeding further infiltration do not change. This hypothesis is sup-

ported by the theory presented by *Cui et al.* [2008], who found that the partial differential equations describing gravity driven and intro-gravel flow driven fine sediment infiltration processes behave similarly. We believe that the relations we developed for sand infiltration into a clean gravel deposit can be used to estimate the potential fraction of silt that can potentially infiltrate a gravel bed already saturated with sand.

[49] As an example of applying our relations to predict infiltration of silt- and clay-sized particles, we present an evaluation of potential silt infiltration into gravel deposits already saturated with sand using field data from Clear Creek. We expect that silt infiltration will be governed by the grain-size distribution of the sand inside the deposit and the grain-size distribution of the infiltrating silt. The estimated potential saturated silt fraction within the sand (i.e., silt volume over the sum of silt and sand volume) can be calculated with equation (6) by replacing the size distribution parameters for gravel with sand (i.e., the bed material creating the pore space) and sand with silt (i.e., the infiltrating sediment). Figure 18 shows the results of applying equation (6) to the field data in Clear Creek, California with altered sediment input parameters, where the infiltrating silt has an assumed geometric mean grain size of 0.02 mm and a geometric standard deviation of 1.5. Similar to how fine sediment infiltrates only a few gravel diameters into a gravel bed, silt infiltration is expected to only extend a few sand diameters into the deposit as demonstrated in Figure 19. The vertical profile of silt infiltration shown in Figure 19 was calculated using equations (6) and (12) and following similar particle size distribution replacements as

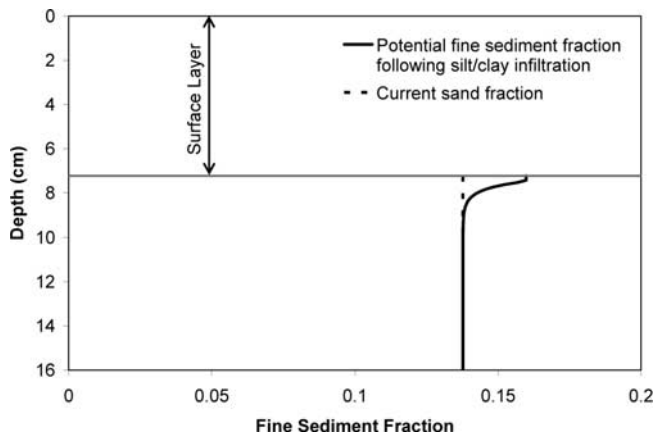


Figure 19. The current sand fraction and potential vertical fine sediment fraction profile following infiltration of silt with a geometric mean grain size of 0.02 mm and a geometric standard deviation of 1.5 for the subsurface sample indicated in Figure 18.

described above for one of the Clear Creek samples. It is important to note, however, these calculations only evaluate the potential increase in the FSF assuming the 0.02 mm silt particles do infiltrate the deposit, but the evaluation does not address the problem as to whether the 0.02 mm silt particles actually infiltrate the bed material, as they are likely transported as part of the suspended load. Field data [e.g., *Shaw and Kellerhals*, 1982] illustrate that the fraction of silt and clay is usually very low (typically <5%) within gravel bed deposits, indicating that it may be difficult for suspended particles to infiltrate a natural sediment deposit.

[50] Two additional issues pertaining to the infiltration of very fine sediment (i.e., silt and clay that typically travel in suspension) cannot be addressed using the experimental data and the relations presented in this paper: 1) how much silt and clay would potentially infiltrate into a gravel bed that is only partially saturated with sand (i.e., where $f < f_s$); and 2) what sized silt and clay particles will infiltrate into the channel bed. These issues are potentially important to dam removal projects, as there may be large volumes of sand, silt and clay released following dam removal.

11. Conclusions

[51] Three flume experimental runs were conducted to examine the infiltration of fine sediment into immobile gravel deposits initially void of fine sediment. Experiments were designed so that each subsequent run increased the fine sediment feed rate by a factor of 10 while reducing the feed duration by a factor of 10, maintaining the same cumulative volume of fine sediment feed over the duration of the run. The two experiments with the slowest feed rates produced approximately the same amount of fine sediment infiltration, while the experiment with the highest fine sediment feed rate resulted in less fine sediment infiltration. Rapid sediment release following dam removal may therefore have the potential benefit of minimizing fine sediment infiltration in addition to the benefit of shorter impact duration. Two relations were developed based on physical

principles and the experimental data that utilize the grain-size distributions of the coarse bed material and infiltrating fine sediment to predict (1) the saturated FSF in the top subsurface layer; and (2) the vertical profile of FSF in the subsurface resulting from fine sediment infiltration into an immobile coarse bed material initially void of fine sediment. In addition to describing fine sediment infiltration into clean gravel deposits, the two relations were used to estimate potential silt infiltration into a gravel bed already saturated with sand, a situation found in the majority of the samples in natural gravel-bedded rivers. The vertical fine sediment relation indicates that substantial fine sediment infiltration occurs only to a depth of a few geometric mean diameters of the bed material, and in the case of silt infiltrating a gravel deposit saturated with sand, substantial infiltration occurs only to a depth of a few sand grains. The two relations suggest that fine sediment infiltration is strongly related to the grain-size distributions of the bed material and the infiltrating fine sediment. A more comprehensive understanding of what sized fine sediment infiltrates into subsurface sediments under different sediment supply and shear stress conditions will greatly extend the utility of the two relations.

Notation

D_g	representative grain size for gravel
D_{gg}	gravel geometric mean grain size
D_s	representative grain size for fine sediment
D_{sg}	geometric mean grain size for the fine sediment
f	fraction of fine sediment in the deposit
\tilde{f}	fine sediment fraction (FSF) normalized with saturated FSF
\tilde{f}_*	weighted-averaged \tilde{f} value
f_{pi}	the i -th predicted \tilde{f} value
f_s	saturated fine sediment fraction (saturated FSF)
k	exponential coefficient in weighting factor equation
N	number of samples
V_g	gravel volume
V_{gp}	pore space in a gravel deposit
V_s	fine sediment volume
V_t	volume of sediment deposit, including pore space
x, y	intermediate variables
z	depth into the deposit, measured from channel surface
\tilde{z}	normalized depth into the deposit
w_i	weighting factor for the i -th sample
α	intermediate parameter
α_1, α_2	coefficients in fine sediment infiltration equations
β, β_1, β_2	coefficients in fine sediment infiltration equations
β'	a first step estimate of β value
ε	Root mean square error of model prediction
γ	regression coefficient
λ_s, λ_g	porosity of fine sediment deposit and gravel deposit, respectively
σ_g	geometric standard deviation
σ_{gg}	gravel geometric standard deviation
σ_{sg}	fine sediment geometric standard deviation
ω	regression coefficient

[52] **Acknowledgments.** Funding for this study was provided by CALFED Ecosystem Restoration Program (Grant No. ERP-02D-P55). The National Center for Earth-surface Dynamics (NCED) based at St. Anthony Falls Laboratory, University of Minnesota, in which the University of California, Berkeley participates and Stillwater Sciences is a partner, provided equipment and technical support. We gratefully acknowledge the assistance and help from Jeremy Venditti, William McDowell, Peter Baker, Evan Lue, Natalie Cabrera, Kurt Yaeger, John Potter, Stuart Foster, Angela Percival, Sayaka Araki, Tami Cosio, Chris Ellis, and Jim Mullen, and the guidance from the project's scientific advisory committee members: Thomas Lisle, Scott McBain, Gary Parker, Kris Vyverberg, and Peter Wilcock. We appreciate the strong support of the past and current Stillwater flume directors: Frank Ligon, Craig Fixler, and Pete Downs. The very helpful and constructive review comments from Tom Lisle, Derek Booth, two anonymous peer reviewers, and the associate editor (Greg Pasternack) to previous drafts were incorporated in this paper.

References

- Allen, J. R. L. (1985), *Principles of Physical Sedimentology*, George Allen & Unwin, London, ISBN 0-04-551095-4.
- Bear, J. (1972), *Dynamics of Fluids in Porous Media*, Dover Publications, Inc., New York, ISBN 0-486-65675-6.
- Beschta, R., and W. L. Jackson (1979), The intrusion of fine sediments into a stable gravel bed, *J. Fish. Res. Board Can.*, 36, 204–210.
- Bjornn, T. C., M. A. Brusven, M. P. Molnau, J. H. Milligan, R. A. Klamt, E. Chacho, and C. Schaye (1977), Transport of granitic sediment in streams and its effects on insects and fish, *Research Technical Completion Report*, Project B-036-IDA, prepared by University of Idaho, Moscow, for Office of Water Research and Technology, U. S. Department of the Interior, Washington, D. C.
- Brusven, M. A., and K. V. Prather (1974), Influence of stream sediments on distribution of macrobenthos, *J. Entomol. Soc. British Columbia*, 71, 25–32.
- Carling, P. A. (1984), Deposition of fine and coarse sand in an open-work gravel bed, *Can. J. Fish. Aquat. Sci.*, 41, 263–270.
- CDWR (California Department of Water Resources) (1994), San Joaquin River tributaries spawning gravel assessment, Stanislaus, Tuolumne, and Merced Rivers, Appendix C: bulk sampling data, surface and subsurface, September.
- CDWR (1995), Sacramento River gravel study - Keswick dam to Cottonwood Creek, memorandum to Stacy Cepello, Environmental Specialist IV, and Koll Buer, Senior Engineering Geologist, October 20.
- Cooper, A. C. (1965), The effect of transported stream sediments on the survival of sockeye and pink salmon eggs and alevin, *Bulletin 18*, International Pacific Salmon Fisheries Commission, New Westminster, British Columbia, Canada.
- Cui, Y. (2007a), The Unified Gravel-Sand (TUGS) model: Simulating sediment transport and gravel/sand grain size distributions in gravel-bedded rivers, *Water Resour. Res.*, 43, W10436, doi:10.1029/2006WR005330.
- Cui, Y. (2007b), Examining the dynamics of grain size distributions of gravel/sand deposits in the Sandy River, Oregon with a numerical model, *River Res. Appl.*, 23(7), 732–751, doi:10.1002/rra.1012.
- Cui, Y., and G. Parker (1998), The arrested gravel front: Stable gravel-sand transitions in rivers, part 2: General numerical solution, *J. Hydraul. Res.*, 36(2), 159–182.
- Cui, Y., and A. Wilcox (2008), Development and application of numerical models of sediment transport associated with dam removal, Chapter 23 in *Sedimentation Engineering: Theory, Measurements, Modeling, and Practice*, ASCE Manual 110, M. Garcia, M. H. Ed., ISBN 978-0784408149, ASCE, Reston, VA.
- Cui, Y., G. Parker, and C. Paola (1996), Numerical simulation of aggradation and downstream fining, *J. Hydraul. Res.*, 34(2), 185–204.
- Cui, Y., C. Braudrick, W. E. Dietrich, B. Cluer, and G. Parker (2006), Dam Removal Express Assessment Models (DREAM), Part 2: Sample runs/sensitivity tests, *J. Hydraul. Res.*, 43(3), 308–323.
- Cui, Y., J. K. Wooster, P. F. Baker, S. R. Dusterhoff, L. S. Sklar, and W. E. Dietrich (2008), Theory of fine sediment infiltration into immobile gravel beds, *Journal of Hydraulic Engineering*, in press, available on line at <http://www.stillwatersci.com/InfiltrationTheoryJHE.pdf> prior to its publication.
- Diplas, P., and G. Parker (1985), Pollution of gravel spawning grounds due to fine sediment, Project Report No. 240, St. Anthony Falls Laboratory, University of Minnesota, Minneapolis, Minnesota, 131 p.
- Einstein, H. A. (1968), Deposition of suspended particles in a gravel bed, *J. Hydraul. Eng.*, 94(HY5), 1197–1205.
- Frostick, L. E., P. M. Lukas, and I. Reid (1984), The infiltration of fine matrices into coarse-grained alluvial sediments and its implications for stratigraphical integration, *J. Geol. Soc. London*, 141, 955–965.
- Gammon, J. R. (1970), The effect of inorganic sediment on stream biota, *Water Pollution Control Research Series*, Grant 18050 DWC 12/70, Water Quality Office of U.S. Environmental Protection Agency, Washington, D. C.
- Graham Matthews and Associates (2003), WY2003 geomorphic monitoring report, Report to Western Shasta Resource Conservation District, Anderson, California.
- Graham Matthews and Associates (2004), WY2004 geomorphic monitoring report, Report to Western Shasta Resource Conservation District, Anderson, California.
- Greig, S. M., D. A. Sear, and P. A. Carling (2005a), The impact of fine sediment accumulation on the survival of incubating salmon progeny: Implications for sediment management, *Sci. Total Environ.*, 344(1–3), 241–258, doi:10.1016/j.scitotenv.2005.02.010.
- Greig, S. M., D. A. Sear, D. Smallman, and P. A. Carling (2005b), Impact of clay particles on the cutaneous exchange of oxygen across the chorion of Atlantic salmon eggs, *J. Fish Biol.*, 66, 1681–1691, doi:10.1111/j.1095-8649.2005.00715.x.
- Greig, S. M., D. A. Sear, and P. A. Carling (2007), A review of factors influencing the availability of dissolved oxygen to incubating salmonid embryos, *Hydrol. Processes*, 21(3), 323–334, doi:10.1002/hyp.6188.
- Groot, C., and L. Margolis (1991), *Pacific salmon life histories*, University of British Columbia Press, Vancouver, 515 p.
- Hausel, D. A., and D. W. Coble (1976), Influence of sand in redds on survival and emergence of brook trout (*Salvelinus fontinalis*), *Trans. Am. Fish. Soc.*, 105, 57–63.
- Hoey, T. B., and R. I. Ferguson (1994), Numerical simulation of downstream fining by selective transport in gravel bed rivers: Model development and illustration, *Water Resour. Res.*, 30, 2251–2260.
- Kondolf, G. M., and M. G. Wolman (1993), The sizes of salmonid spawning gravel, *Water Resour. Res.*, 29, 2275–2285.
- Koski, K. V. (1966), The survival of coho salmon (*Oncorhynchus kisutch*) from egg deposition to emergence in three Oregon coastal streams, Master's Thesis, Oregon State University, Corvallis.
- Lauck, T. (1991), A simulation model for the infiltration of sediment into spawning gravel, Master's Thesis, Humboldt State University, August.
- Lisle, T. E. (1989), Sediment transport and resulting deposition in spawning gravels, North Coastal California, *Water Resour. Res.*, 25(6), 1303–1319.
- Parker, G. (1990), Surface-based bedload transport relation for gravel rivers, *J. Hydraul. Res.*, 28(4), 417–436.
- Parker, G., and A. J. Sutherland (1990), Fluvial armor, *J. Hydraul. Res.*, 28(5), 529–544.
- Phillips, R. W., R. L. Lantz, E. W. Claire, and J. R. Moring (1975), Some effects of gravel mixtures on emergence of coho salmon and steelhead trout fry, *Trans. Am. Fish. Soc.*, 104, 461–466.
- Rathburn, S. L., and E. E. Wohl (2001), One-dimensional sediment transport modeling of pool recovery along a mountain channel after a reservoir sediment release, *Reg. Rivers Res. Manage.*, 17, 251–273, doi:10.1002/rra.617.
- Rohn, A. D. (1997), Intergravel Sedimentation: A Vertical Stratified Infiltration Model (Physical), Master's Thesis, Humboldt State University, Arcata, California, 68 p.
- Schälchli, U. (1992), The clogging of coarse gravel river beds by fine sediment, *Hydrobiologia*, 235/236, 189–197.
- Seal, R., G. Parker, C. Paola, and B. Mullenbach (1995), Laboratory experiments on downstream fining of gravel, narrow channel Runs 1 through 3: Supplemental methods and data, *External Memorandum No. 239*, St. Anthony Falls Laboratory, University of Minnesota, Minneapolis, Minnesota, March, 477 p.
- Sear, D. A., P. A. Carling, and S. M. Grieg (2005), Fine sediment accumulation in spawning gravels and the effects on interstitial flow, in *Fifth International Symposium on Ecohydraulics: Aquatic Habitats: Analysis & Restoration*, edited by D. J. Lastra and P. V. Martinez, pp. 808–812, IAHR, Madrid.
- Shaw, J., and R. Kellerhals (1982), The composition of recent alluvial gravels in Alberta River beds, *Bulletin 41*, Alberta Research Council, Edmonton, Alberta, Canada.
- Sutherland, D. G., M. Hansler-Ball, S. J. Hilton, and T. E. Lisle (2002), Evolution of a landslide-induced sediment wave in the Navarro River,

- California, *GSA Bull.*, 114(8), 1036–1048, doi:10.1130/0016-7606(2002)114<1036:EOALIS>2.0.CO;2.
- Toro-Escobar, C. M., G. Parker, and C. Paola (1996), Transfer function for the deposition of poorly sorted gravel in response to streambed aggradation, *J. Hydraul. Res.*, 34(1), 35–53.
- Walling, D. E. (1999), Linking land use, erosion and sediment yields in river basins, *Hydrobiologia*, 410, 223–240, doi:10.1023/A:1003825813091.
-
- Y. Cui, S. R. Dusterhoff, M. Malko, and J. K. Wooster, Stillwater Sciences, 2855 Telegraph Ave. Suite 400, Berkeley, CA 94705, USA. (yantao@stillwatersci.com)
- W. E. Dietrich, Department of Earth and Planetary Science, University of California, Berkeley, CA, USA.
- L. S. Sklar, Department of Geosciences, San Francisco State University, San Francisco, CA, USA.